



Comprehensive Validation of Skeletal Mechanism for Turbulent Premixed Methane–Air Flame Simulations

Stefano Luca*

King Abdullah University of Science and Technology, Thuwal 23955-6900, Saudi Arabia

Ashraf N. Al-Khateeb[†]

Khalifa University, Abu Dhabi 127788, United Arab Emirates

Antonio Attili[‡]

RWTH Aachen University, 52056 Aachen, Germany

and

Fabrizio Bisetti[§]

University of Texas at Austin, Austin, Texas 78712

DOI: 10.2514/1.B36528

A new skeletal mechanism, consisting of 16 species and 72 reactions, has been developed for lean methane–air premixed combustion from the GRI-Mech 3.0. The skeletal mechanism is validated for elevated unburnt temperatures (800 K) and pressures up to 4 atm, thereby addressing realistic gas turbine conditions. The skeletal mechanism is obtained by applying the directed relation graph method and performing sensitivity analysis on the detailed mechanism. The mechanism has been validated for flame speed and flame structure in a wide range of conditions and configurations. A good agreement between the skeletal mechanism and GRI-3.0 was obtained. The configurations considered include one-dimension laminar premixed flames, laminar non-premixed counterflow burners, and two- and three-dimensional unsteady configurations with variations of temperature, pressure, and composition. The skeletal mechanism allows for the inclusion of accurate finite rate chemistry in large-scale direct numerical simulations of lean turbulent premixed flames. In a large-scale direct numerical simulation, the use of the skeletal mechanism reduces the memory requirements by more than a factor of 3 and accelerates the simulation by a factor of 7 compared with the detailed mechanism. The skeletal mechanism is suitable for unsteady three-dimensional simulations of methane turbulent premixed, non-premixed, and globally lean partially premixed flames and is available as supplementary material.

I. Introduction

IN THE current era of increasing environmental concerns, there is considerable demand to improve efficiency and reduce emissions of the next generation combustion devices. Fuel-flexible designs that can burn both conventional and alternative fuels are also desired. Because computational modeling assists in the design of engines and combustors for aerospace, transportation, and energy applications, accurate prediction of fuel combustion and pollutant emissions requires comprehensive detailed reaction mechanisms.

In many practical applications for power generation, such as stationary gas turbines, lean premixed combustion offers the key advantages of high thermal efficiency and low NO_x emissions. Lean premixed combustion presents differences with respect to stoichiometric conditions: lean flames tend to be thicker and propagate slower due to the lower flame temperature. In principle, a thicker flame is more prone to be affected by the smallest turbulent structures and the turbulent velocity fluctuations can have a higher impact due to the lower flame speed.

Thanks to the increase of computational resources, direct numerical simulation (DNS) has become an important tool to study turbulent combustion problems and provides valuable insight into the

physics of flame–turbulence interaction [1]. Despite rapid advancements in computing power, it is generally prohibitive to include detailed reaction mechanisms in large-scale simulations due to the prohibitive CPU time and memory requirements, because the computational cost of chemistry scales by the third power of the number of species in the worst case when factorizing the Jacobian [2,3]. In addition, the wide range of timescales [$\mathcal{O}(10^{-9}$ – 10^{-3} s)] and the nonlinear coupling between species and reactions induces stiffness in the governing equations [2]. Because of these computational demands, the reduction of large mechanisms is necessary to facilitate practical simulations using realistic chemistry with modern computational tools.

Skeletal and reduced mechanisms based on few steps were first derived by Peters [4]. Peters introduced, in his chemical kinetics, the coupling between a reduced number of elementary steps and analytical relations for the intermediate species obtained via quasi-steady-state and equilibrium hypotheses [5–8].

Theoretical analysis of the inner structure of laminar flames and reaction zones were conducted using these simple mechanisms [9,10]. Then, further chemical schemes ready for turbulent flow simulations were derived by many groups (see, for instance, [11–14]).

Two main types of reduced kinetic schemes can be found in the literature for simulating turbulent flames: Global schemes, the first type, are based on a few steps in which only major species are involved and the constants of these global chemical rates are adjusted to match experimental measurements or reference responses obtained with a detailed chemistry that was previously validated. Reduced schemes, the second type, are also based on a few steps, but have been obtained from a systematic downsizing of a detailed kinetics. Numerical procedures have been developed to understand the direct and indirect impact of species and elementary reactions on a given target set of chemical species, to be reproduced by the reduced scheme [14–19]. The species and reactions with the least influence on the target species may then be removed. For both types, a target model

Received 2 November 2016; revision received 10 April 2017; accepted for publication 13 May 2017; published online 31 July 2017. Copyright © 2017 by the American Institute of Aeronautics and Astronautics, Inc. All rights reserved. All requests for copying and permission to reprint should be submitted to CCC at www.copyright.com; employ the ISSN 0748-4658 (print) or 1533-3876 (online) to initiate your request. See also AIAA Rights and Permissions www.aiaa.org/randp.

*Ph.D. Student, Clean Combustion Research Center, Mechanical Engineering Department, Member AIAA.

[†]Assistant Professor, Department of Aerospace Engineering, Member AIAA.

[‡]Researcher, Institute for Combustion Technology, Member AIAA.

[§]Assistant Professor, Department of Aerospace Engineering and Engineering Mechanics, Member AIAA.

problem should be chosen to probe the chemical response along representative evolutions of chemistry from fresh to burnt gases [20].

The purpose of the reduction is to obtain a skeletal mechanism to be used in large direct numerical simulations of lean methane–air mixture at 800 K. One of the constraints in a large-scale simulation is related to the number of species in the chemical mechanism. The costs of performing DNS increases more than linearly with the number of species. The cost is related to the solution of the transport equations for the reactive scalars and to the computation of the reaction rate due to chemical reactions. Because the integration of the system of equations governing reactive flows is often achieved with an implicit time integration scheme, a reduction of the number of species produces a significant reduction in computational cost.

The objective of this study is the validation of a rather small chemical mechanism to be applied in large-scale direct numerical simulations of lean premixed combustion. The validation was performed over a wide range of different problems in one dimension and also in more realistic configurations that feature unsteadiness and two- and three-dimensionality. The most detailed validation was performed for premixed flames, because this new skeletal chemical kinetic mechanism has been developed to be used in direct numerical simulations of lean premixed methane–air flame. The skeletal mechanism consist of 16 species and 72 reversible reactions and is obtained from the application of the directed relation graph (DRG) methodology and sensitivity analysis on the GRI-3.0 detailed mechanism. The mechanism has been validated for flame speed and flame structure for the target unburnt mixture conditions and good agreement was obtained. The skeletal reaction mechanism and the thermodynamic and transport data are available as an electronic supplement to this manuscript.

II. Methodology

The reduction is accomplished through the sequential application of the DRG framework [16] and sensitivity analysis to the GRI-3.0 detailed mechanism [21], which contains 53 species and 325 reactions. The DRG method, originally proposed by Lu and Law [16,22,23], uses a directed graph to map the coupling of species and consequently find candidate species to be removed. Whether the species are removed or not depends on user-defined target species and an error threshold.

The reduction was conducted by sampling a set of thermochemical states in a freely propagating one-dimensional laminar flame. The reaction states were sampled under atmospheric pressure, lean conditions, and unburnt temperature of 800 K. The product species

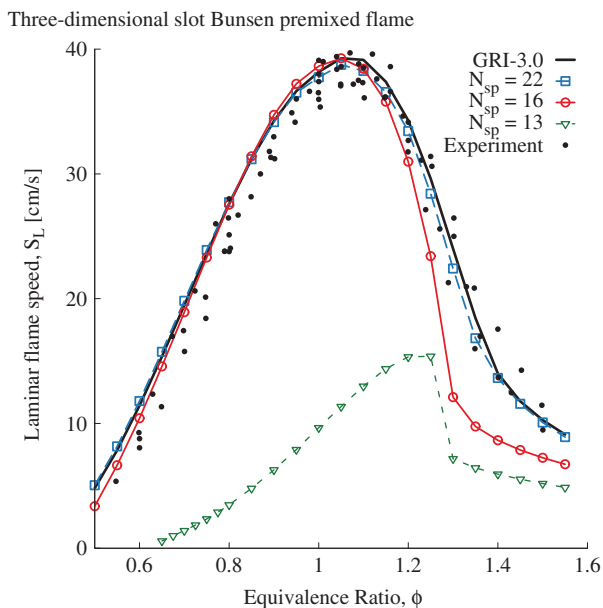


Fig. 1 Laminar flame speed comparison for a methane–air flame with unburnt temperature of 300 K and 1 atm.

Table 1 Species included in the three skeletal mechanisms, including the proposed one with 16 species

Species	$N_{sp} = 13$	$N_{sp} = 16$	$N_{sp} = 22$
CH ₄	✓	✓	✓
O ₂	✓	✓	✓
N ₂	✓	✓	✓
CO ₂	✓	✓	✓
H ₂ O	✓	✓	✓
CO	✓	✓	✓
OH	✓	✓	✓
O	✓	✓	✓
H	✓	✓	✓
H ₂	✓	✓	✓
HO ₂	✓	✓	✓
CH ₃	✓	✓	✓
CH ₂ O	✓	✓	✓
HCO	— —	✓	✓
CH ₂	— —	✓	✓
CH ₂ (S)	— —	✓	✓
CH	— —	— —	✓
H ₂ O ₂	— —	— —	✓
CH ₃ O	— —	— —	✓
C ₂ H ₄	— —	— —	✓
C ₂ H ₅	— —	— —	✓
C ₂ H ₆	— —	— —	✓

CO₂ was used as a target in the reduction process, and an error threshold, following Lu and Law’s [16] definition, of 0.55 was used. Sensitivity analysis with the software CHEMKIN PRO was performed on states obtained from a premixed, freely propagating flame at the condition of 800 K and 1 atm to validate the results obtained from DRG. No further reduction was achieved.

It is found that 16 species is the minimum number of species required to obtain a skeletal mechanism with satisfactory predictions of key quantities such as laminar flame speed, laminar flame thickness, peak temperature, and species mass fractions. A further reduction was attempted without obtaining acceptable results. Figure 1 shows the comparison of the laminar flame speed computed with three skeletal mechanisms and with the complete GRI-3.0: Although increasing the number of species would produce results closer to the laminar flame speed of GRI-3.0, the results with 16 species are satisfactory. Also shown are experimental data available in the literature [24–27]. Table 1 shows the species of the three skeletal mechanisms used in Fig. 1, including the final skeletal mechanism with 16 species. The species that were removed and not considered in the final skeletal mechanism are listed in the supplementary material.

III. Validation

A detailed and comprehensive validation of the skeletal mechanism is performed comparing temperature and species mass fractions computed with the detailed mechanism GRI-3.0 and the skeletal mechanism in configurations of increasing complexity, ranging from one-dimensional laminar flames to three-dimensional turbulent jets. The results are obtained employing the PREMIX code [28] in one-dimensional unstretched laminar premixed flames and the FlameMaster package [29] in one-dimensional counterflow configurations. Validations in a two-dimensional configuration are presented for both premixed and non-premixed unsteady flames. Finally, a large direct numerical simulation of a turbulent methane–air flame in a slot Bunsen burner configuration was performed. The two- and three-dimensional simulations are performed using the in-house code NGA [30].

A. One-Dimensional Unstretched Premixed Laminar Flames

The skeletal and detailed mechanisms are compared for laminar one-dimensional premixed flames computed with PREMIX [31]. The code solves one-dimensional, unstretched, premixed flames with support for thermodynamics, transport, and kinetics data and relies

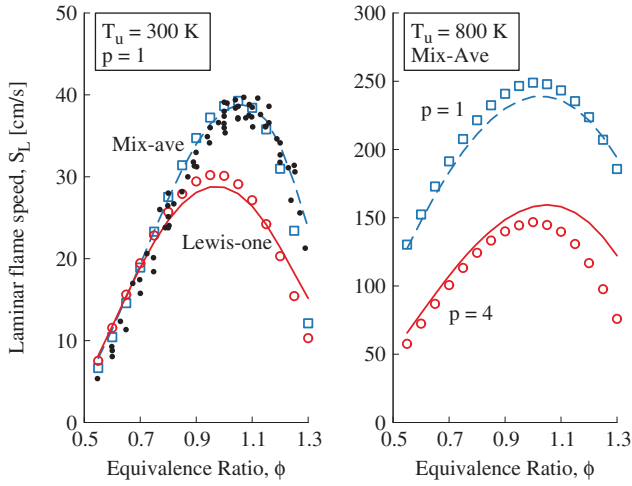


Fig. 2 Laminar flame speed for the detailed (lines) and skeletal (open symbols) mechanisms.

on a boundary value problem solver [28]. The computed laminar flame speed as a function of the equivalence ratio of the mixture is shown in Fig. 2. The results are shown for two different transport models (mixture-averaged [32] and unity Lewis numbers) at two different unburnt gas temperature ($T_u = 300$ and 800 K). The laminar flame speed is also compared with experimental data available in the literature [24–27].

The laminar flame speed computed with the skeletal mechanisms is very close to the one computed with the detailed mechanisms up to $\phi = 1.1$ and the difference is comparable with the scatter in the experimental results. At lean conditions, excellent agreement is found for different initial temperatures, pressures, and transport models. At larger equivalence ratios, the difference is greater.

The comparison of the thermal flame thickness, defined as

$$\delta_L = \frac{T_b - T_u}{|dT/dx|_{\max}} \quad (1)$$

where T_b and T_u are the burnt and the unburnt temperature, respectively, is shown in Fig. 3 for different initial temperatures (300 and 800 K) and pressures (1 and 4 atm) with a mixture-averaged transport model. The main target application of the skeletal mechanism is a set of direct numerical simulations of turbulent premixed flames. In turbulent premixed flames, the ratio between the laminar flame thickness and the characteristic scales of the turbulent field is of primary importance; in addition, the effects of turbulence on the local thickness of the flame is usually a subject of

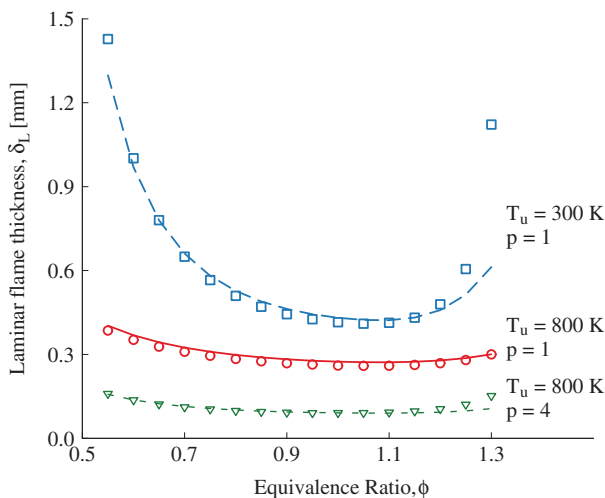


Fig. 3 Laminar flame thickness for the detailed (lines) and skeletal (symbols) mechanisms.

investigation. Therefore, it is important for the skeletal mechanism to compute the flame thickness accurately. The agreement is excellent for lean mixtures and up to $\phi = 1.2$ in the range of temperatures and pressures of interest.

An analysis of the temperature and species mass fraction profiles at 4 atm and equivalence ratio 0.7 is presented in Fig. 4. The temperature and the mass fraction of major and radical species show very good agreement. Values at equilibrium for the skeletal mechanism are within a few percent of those computed with the detailed mechanism (not shown).

The dependence on pressure has been investigated and results for selected quantities are presented in Fig. 5. Laminar flame speed and thickness, and peak OH and H mass fractions, are shown for different equivalence ratios at lean conditions. The results computed with the skeletal mechanism (Ske) agree well with those computed using GRI-3.0 (Det) for the range of pressure between 1 and 16 atm. The discrepancy in the laminar flame speed increases as pressure increases, whereas the other quantities show a good agreement over the entire range. At 4 atm, the laminar flame speed from the skeletal mechanism falls within 15% for equivalence ratios between 0.5 and 1. Overall, the comparison for premixed laminar configuration shows very good agreement for the target conditions and for the range of equivalence ratios and pressures investigated.

B. One-Dimensional Non-Premixed Laminar Flames

Non-premixed one-dimensional steady flames are computed using the FlameMaster code [29] to obtain a more comprehensive validation. The configuration used is a canonical counterflow flame routinely used in experiments [33,34] and to assemble reduced models based on chemistry tabulation [35].

A set of flamelets was obtained by performing simulations at different stoichiometric scalar dissipation rates χ_{st} with constant Lewis number approximation for the transport model. The values of the Lewis numbers used are available as supplementary material. Results for three flamelets at stoichiometric scalar dissipation equal to $\chi_{st} = 0.01, 1, \text{ and } 80 \text{ s}^{-1}$ are shown in Fig. 6. The temperature and the mass fractions of H_2O , OH, and H show excellent agreement. Good agreement was also found for all other species (not shown).

The maximum temperature and the peak H_2O , CO, CO_2 , OH, O, and H mass fractions as a function of the stoichiometric scalar dissipation rates are presented in Fig. 7 for the two mechanisms. The results are shown for a wide range of stoichiometric scalar dissipation rates, up to flame extinction. The reduced mechanism predicts the peak of temperature and species mass fraction as function of the scalar dissipation correctly. In addition, the value of scalar dissipation at extinction, a very important parameter, is the same for both mechanisms. Overall, the comparison in the one-dimensional non-premixed case shows good results.

C. Unsteady Two-Dimensional Premixed Flame

In this section, we consider a two-dimensional unsteady spatially developing slot Bunsen flame. The inlet condition is a premixed methane–air mixture at equivalence ratio $\phi = 0.7$ with a temperature of the unburnt mixture of 800 K and pressure of 1 atm. The coflow is made of combustion products of the same methane–air mixture at the equilibrium thermochemical state.

The gas-phase hydrodynamics are modeled with the reactive unsteady Navier–Stokes equations in the low Mach number limit and solved with the in-house code NGA [30]. The species obey the ideal gas equation of state and all transport properties are computed with a mixture-average approach [32].

The velocity imposed at the inlet is $U = 60 \text{ m/s}$ for the central jet and 15 m/s for the coflow. The slot width is $H = 1.2 \text{ mm}$ and the domain is $18 \times 12H$. The resolution is $\Delta x = \Delta y = 20 \mu\text{m}$ near the center of the domain and the grid is stretched along the y direction, resulting in $1080 \times 514 = 550 \times 10^3$ grid points. Statistics are collected over 100 time instants after the flowfield is statistically stationary.

The mean temperature and the mean mass fractions conditioned on the progress variable C are shown in Fig. 8 at a specific axial location

Premixed freely propagating flame $\phi=0.7$, $T_u=800$ K, $p=4$ atm

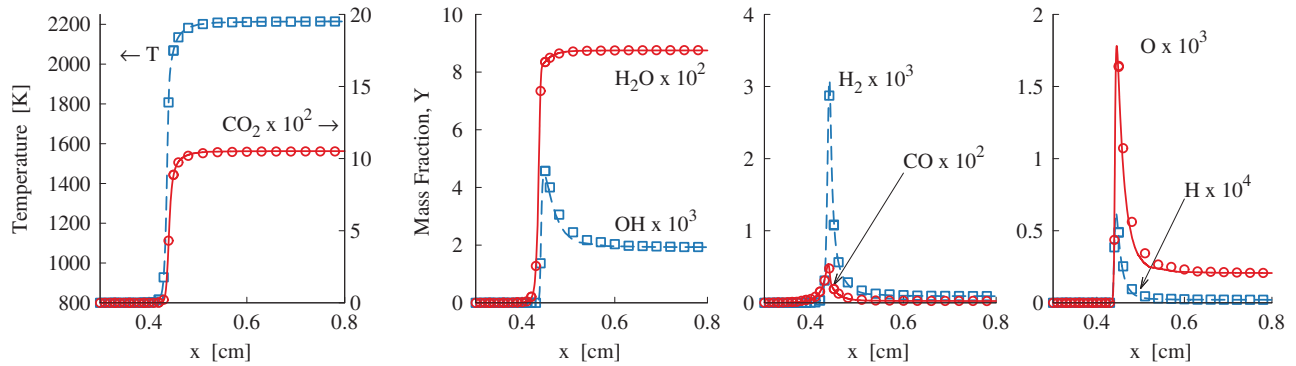


Fig. 4 Profiles of temperature, and selected species mass fractions for the detailed (lines) and the skeletal (symbols) mechanisms.

Premixed freely propagating flame $T_u=800$ K

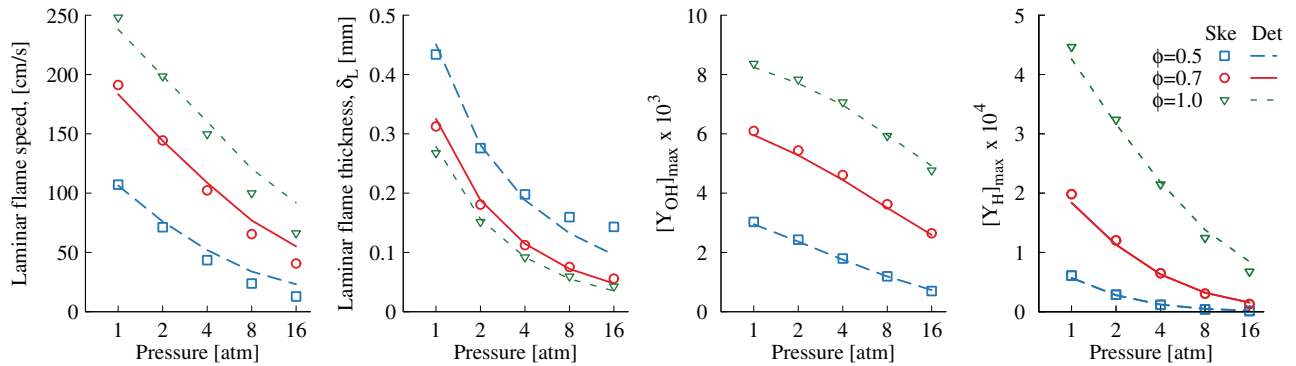


Fig. 5 Pressure dependence of selected quantities.

Non-Premixed one-dimensional flame

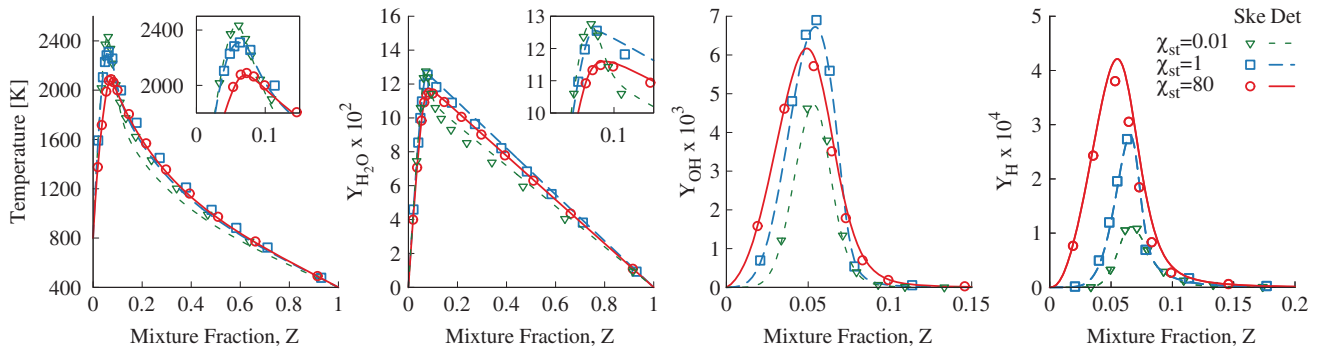


Fig. 6 Temperature and selected mass fractions profiles. Insets show details of the regions near the peak values.

($x \approx 11$ mm). A progress variable is defined using the molecular oxygen mass fraction Y_{O_2} :

$$C = 1 - \frac{Y_{O_2} - Y_{O_{2b}}}{Y_{O_{2u}} - Y_{O_{2b}}} \quad (2)$$

where $Y_{O_{2u}}$ and $Y_{O_{2b}}$ are the oxygen mass fractions in the unburnt and in the burnt gases, respectively. The conditional means computed with the two mechanisms show a very good agreement. This configuration contributes to validate the response of the mechanism in unsteady premixed problems, showing virtually no difference between the skeletal and detailed model. The same agreement between the two data sets is found at several other axial locations (not shown).

D. Unsteady Two-Dimensional Non-Premixed Flame

A two-dimensional, time-evolving jet is used to test the performance of the skeletal mechanism in an unsteady non-premixed

flame. The configuration is similar to that employed by Bisetti et al. [36]. The two-dimensional computational domain consists of a square of size L . Periodic boundary conditions are applied in both crosswise x and streamwise y directions, resulting in a constant volume system. The simulation is initialized with a strip of fuel surrounded by oxidizer. The fuel stream consists of pure methane at 400 K, whereas the oxidizer stream consists of air (21% oxygen and 79% nitrogen) at 800 K. The simulation is performed at 1 atm.

The reactive scalar fields are initialized as follows. The temperature and chemical species mass fractions are taken from a one-dimensional flamelet solution and mapped from mixture fraction space into the horizontal coordinate, according to the mixture fraction spatial profile:

$$Z(x) = \frac{1}{4} \left(1 + \tanh \left[\frac{L + h_z + \delta_z - 2x}{\delta_z} \right] \right) \cdot \left(1 + \tanh \left[\frac{-L + h_z + \delta_z + 2x}{\delta_z} \right] \right) \quad (3)$$

where δ_z is equal to the inverse of the maximum gradient of Z and controls the scalar dissipation rate at stoichiometry. The fuel strip is indicated by h_z .

The one-dimensional flamelet solution is obtained at a prescribed stoichiometric scalar dissipation rate $\chi_{st} = 10 \text{ s}^{-1}$. The scalar dissipation rate imposed to compute the one-dimensional flamelet solution matches the scalar dissipation rate in the two-dimensional computational domain along the crosswise direction at the onset of the simulation. The velocity field is initialized with isotropic turbulence of prescribed fluctuations u' and integral length L_{11} according to the procedure outlined by Passot and Pouquet [37]. The parameters of the simulation are summarized in Table 2. More information about the configuration and the initialization may be found in Bisetti et al. [36].

The simulation is advanced in time for 1500 steps with a constant time step $\Delta t = 1 \mu\text{s}$ for a total simulation time of 1.5 ms. The same

$N_x \times N_y$, mm	600 × 600	$\Delta x, \Delta y, \mu\text{m}$	25
L	15	$\Delta t, \mu\text{s}$	1
h_z	10	$t_{\text{fin}}, \text{ms}$	1.5
δ_z	2	$u', \text{cm/s}$	75

simulation is performed with both mechanisms, and comparisons are presented in Fig. 9. The mean temperature conditioned on mixture fraction Z for the skeletal mechanism is in perfect agreement with the one of the detailed mechanism. Some differences are found for major species and radical mass fractions. Comparing these results with the findings in the one-dimensional steady configuration (see Fig. 6), it appears that the agreement between the two mechanisms for H_2O and OH is degraded by the unsteady nature of the simulation. Conversely, the agreement for temperature, CO_2 , and O remains good.

E. Three-Dimensional Direct Numerical Simulation

Finally, the detailed and skeletal mechanisms are employed in a three-dimensional direct numerical simulation of a turbulent premixed methane–air flame in a slot Bunsen burner configuration. This configuration is the most relevant to the intended use of the mechanism. The configuration is similar to the one used by Sankaran et al. [38] and the same used by the authors of this paper in a previous study [39].

The flame configuration is a slot jet surrounded by a coflow of combustion products. This arrangement is similar to piloted turbulent premixed flames used in experiments [40]. The jet consists of a methane–air mixture with equivalence ratio $\phi = 0.7$ at 800 K. The temperature and species concentration in the coflow correspond to the equilibrium state of the reactants. The simulations are performed at 4 atm. The bulk jet velocity is $U = 100 \text{ m/s}$, whereas the coflow has a uniform velocity of $U_c = 15 \text{ m/s}$. The jet Reynolds number, based on the slot width and the jet bulk velocity, is $U_b H / \nu = 5600$. The domain size expressed in terms of the slot width $H = 1.2 \text{ mm}$ is $24 \times 16 \times 4.2H$. The grid is uniform in all three directions, with a resolution of $20 \mu\text{m}$ resulting in 350 million grid points. The flow is periodic in the spanwise z direction, open boundary conditions are prescribed at the outlet in the streamwise x direction, and no-slip conditions are imposed at the boundaries in the crosswise y direction. More information on the configuration may be found in Luca et al. [39].

The mesh size results in a spatial resolution below twice the minimum average Kolmogorov scale and the flame fronts are resolved with approximately six points. The flame is initially planar near the jet nozzle and shows significant evolution and wrinkling with downstream distance. Downstream, the flame is strongly wrinkled and the wrinkling occurs at various scales, indicating transition to turbulence. Figure 10 shows an instantaneous two-dimensional contour plot of the temperature field and the flame location as an isolate at $T = 1800 \text{ K}$.

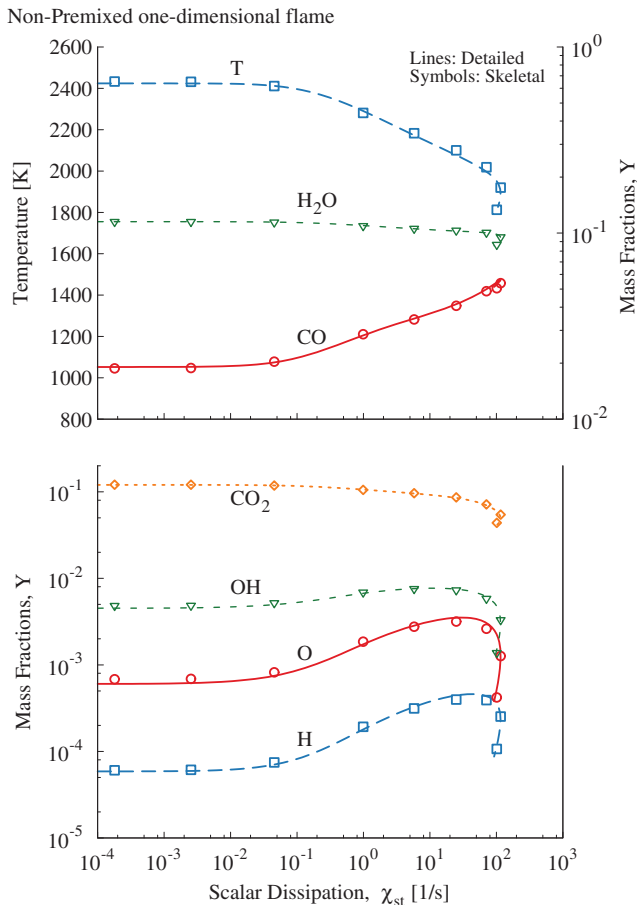


Fig. 7 Maximum values of selected quantities for a range of χ_{st} obtained using the FlameMaster code [29].

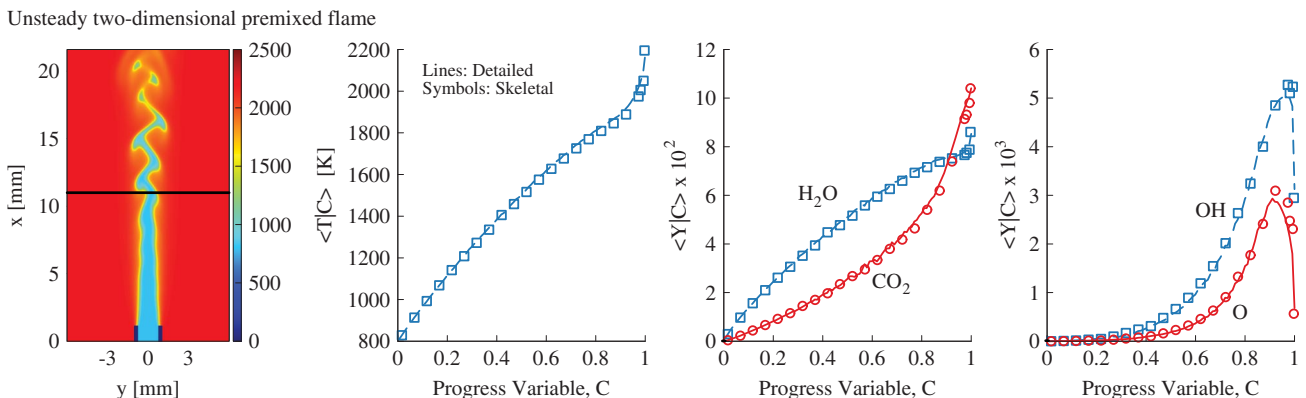


Fig. 8 Temperature contour and conditional mean of selected quantities, computed at the location marked with the horizontal line.

Unsteady two-dimensional non-premixed flame

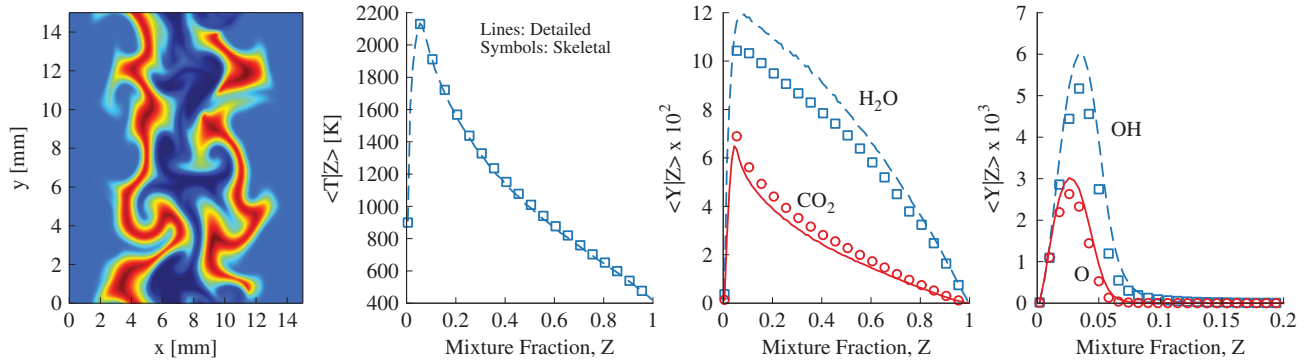


Fig. 9 Instantaneous contour plot of temperature at $t = 0.6$ ms and conditional mean of temperature and selected mass fractions.

Three-dimensional slot Bunsen premixed flame

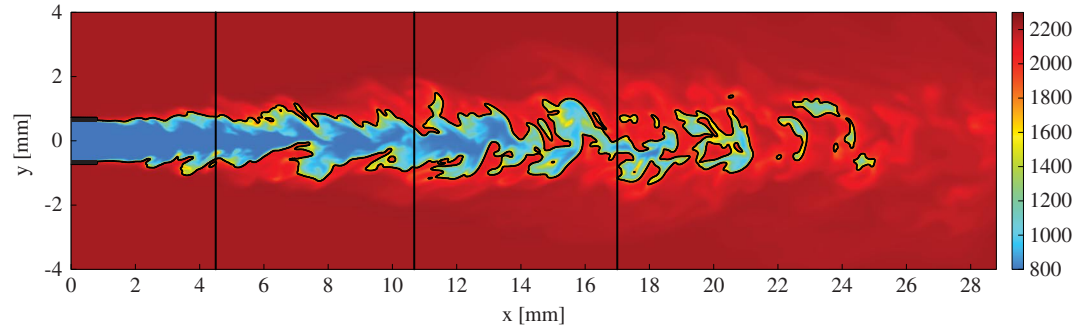


Fig. 10 Instantaneous temperature contour plot. An isoline of temperature identifies the flame location. Vertical black lines mark axial locations at which results are presented.

Figure 11 shows the radial profiles of mean axial velocity U normalized with U_b , velocity fluctuation u'/S_L , and the mean temperature at three axial locations shown in Fig. 10. Probability density functions (PDFs) of the magnitude of the temperature gradient are also shown. A very good agreement is found for all quantities.

Because of the presence of mean shear, the turbulent scales and statistics are not spatially homogeneous in the axial direction. Results are presented at three axial locations representative of the general evolution of the fields.

Conditional means of selected species mass fractions conditioned on temperature are presented in Fig. 12. A very good agreement is found for most of the species. The worst comparison is observed for the mass fraction of the H radical.

Very good agreement is found also in the PDFs of species mass fractions conditioned on three values of temperature, shown in Fig. 13. Results from the two mechanisms are very similar, with

minor differences that can be attributed to convergence. In particular, the most probable values match for the two mechanisms.

Overall, the results obtained with the skeletal mechanism agree very well with those obtained with the detailed mechanism for all variables considered. A similar agreement is found for all other variables that are not shown here.

At this point, it is worthwhile to discuss the implications of the reduction of the number of species in the context of a large-scale DNS of turbulent combustion. First, the memory requirements are reduced by a factor of $53/16 \approx 3$. Second, the computational time required to advance the solution over one time step decreases from 70 to 10 s, when performed on the Cray XC40 supercomputer “Shaheen” on 16,384 cores, thereby bringing a speed-up by a factor of 7. Note that these savings are due to the reduced number of scalars to be transported (10%) and the reduction in the time required to integrate the chemical reactions and compute the transport properties for the mixture (90%).

Three-dimensional slot Bunsen premixed flame

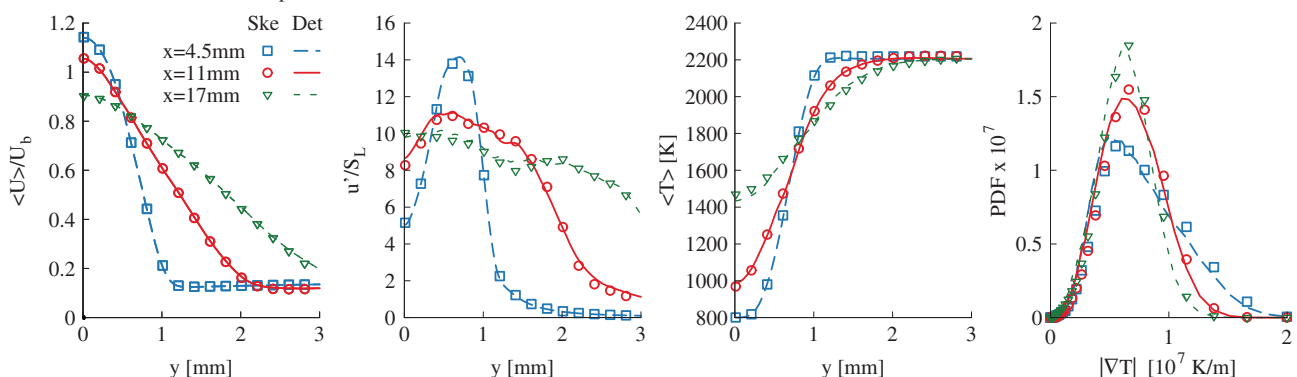


Fig. 11 Mean radial profiles of selected quantities and PDF of temperature gradient conditioned at $T = 1800$ K.

Three-dimensional slot Bunsen premixed flame

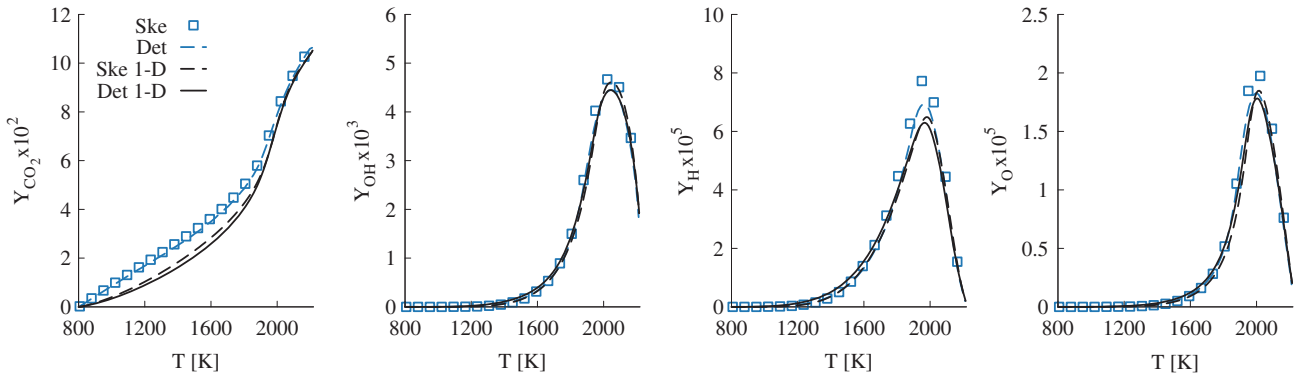
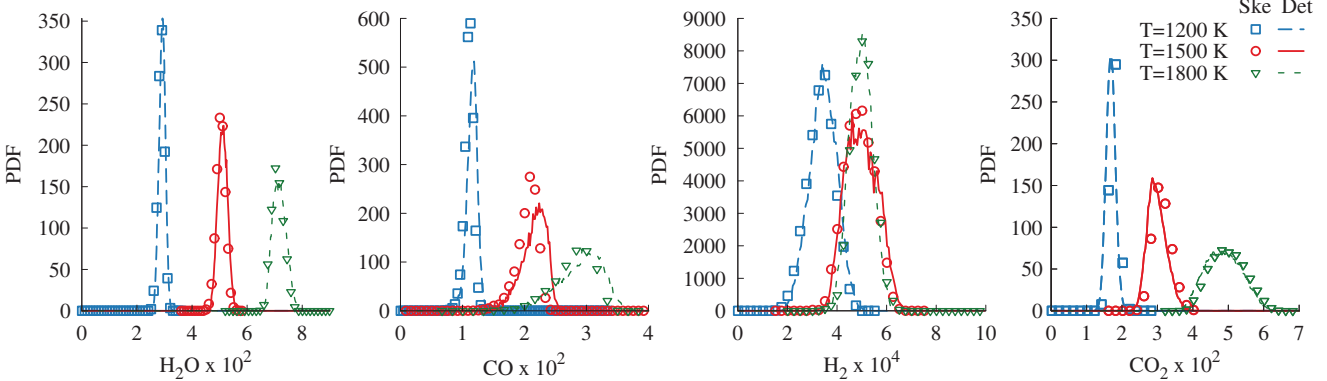


Fig. 12 Conditional mean of selected species mass fraction. Black lines show one-dimensional (1-D) laminar solutions.

Three-dimensional slot Bunsen premixed flame

Fig. 13 PDF of selected species mass fractions conditioned on $T = 1200, 1500,$ and 1800 K.

IV. Conclusions

In this work, a new skeletal mechanism for lean premixed methane-air combustion has been developed and validated. The mechanism is meant to be applied to a campaign of large-scale direct numerical simulations of turbulent premixed combustion at elevated pressure. The detailed mechanism is the well-known GRI-Mech 3.0 mechanism. Upon reduction, the skeletal mechanism obtained consists of 16 species, including molecular nitrogen and 72 reversible reactions.

A comprehensive validation was performed by comparing key quantities in two- and three-dimensional simulations of unsteady flames using the two mechanisms. To confirm the validity of the reduction, the most detailed validation was performed for premixed flames, given the targets. This validation includes one-dimensional unstretched laminar premixed and non-premixed flames, two-dimensional unsteady slot premixed and non-premixed flames, and a three-dimensional turbulent slot premixed flame.

In one-dimensional cases, canonical quantities are compared for the two mechanisms. Laminar flame speed, flame thickness, temperature, and species profiles in physical space, computed for different unburnt temperatures, pressures, and equivalence ratios, show excellent agreement at the conditions investigated. Even if the skeletal mechanism was developed for premixed combustion, validation in non-premixed cases was performed to widen the scope. The results for flames in a one-dimensional counterflow configuration obtained with the skeletal mechanism match the results obtained with the detailed mechanism for a wide range of values of scalar dissipation rate.

The skeletal mechanism is also tested in two-dimensional configurations, premixed and non-premixed. Conditional statistics of temperature and species mass fractions are compared for the two mechanisms and excellent agreement is found. In the case of the non-premixed flame, the unsteadiness and inhomogeneity due to the fluctuating initial velocity field appears to degrade the performance of the skeletal mechanism.

Finally, a three-dimensional direct numerical simulation of a turbulent slot Bunsen flame is considered. No difference is found in the flowfield, showing that transport of momentum is not affected. Good agreement is also found for the species conditional means and probability density functions.

This study suggests that the skeletal mechanism is able to retain accuracy for all quantities of interest. Because of a much lower number of species, the skeletal mechanism results in memory savings by a factor of $53/16 \approx 3$ and in computational time by a factor of 7 in the case of a direct numerical simulation of a turbulent premixed slot flame in three dimensions.

The skeletal mechanism is suitable for use in unsteady three-dimensional simulations of methane turbulent premixed, non-premixed, and globally lean partially premixed flames and is available as supplementary material.

Acknowledgments

The research reported in this publication was supported by funding from King Abdullah University of Science and Technology. We acknowledge valuable support from the Supercomputing Laboratory in the form of computational time on the CRAY XC40 Shaheen supercomputer available at King Abdullah University of Science and Technology.

References

- [1] Chen, J. H., "Petascale Direct Numerical Simulation of Turbulent Combustion-Fundamental Insights Towards Predictive Models," *Proceedings of the Combustion Institute*, Vol. 33, No. 1, 2011, pp. 99–123. doi:10.1016/j.proci.2010.09.012
- [2] Lu, T., and Law, C. K., "Toward Accommodating Realistic Fuel Chemistry in Large-Scale Computations," *Progress in Energy and Combustion Science*, Vol. 35, No. 2, 2009, pp. 192–215. doi:10.1016/j.pecs.2008.10.002

- [3] Bisetti, F., "Integration of Large Chemical Kinetic Mechanisms via Exponential Methods with Krylov Approximations to Jacobian Matrix Functions," *Combustion Theory and Modelling*, Vol. 16, No. 3, 2012, pp. 387–418.
doi:10.1080/13647830.2011.631032
- [4] Peters, N., "Systematic Reduction of Flame Kinetics Principles and Details," *Dynamics of Reactive Systems. Part 1: Flames*, Progress in Astronautics and Aeronautics, AIAA, Washington, D.C., 1988, pp. 67–86.
- [5] Peters, N., "Flame Calculations with Reduced Mechanisms-An Outline," *Reduced Kinetic Mechanisms for Applications in Combustion Systems*, Springer-Verlag, New York, 1993, pp. 3–14.
- [6] Griffiths, J., "Reduced Kinetic Models and Their Application to Practical Combustion Systems," *Progress in Energy and Combustion Science*, Vol. 21, No. 1, 1995, pp. 25–107.
- [7] Goussis, D. A., and Maas, U., "Model Reduction for Combustion Chemistry," *Turbulent Combustion Modeling*, Springer-Verlag, Berlin, 2011, pp. 193–220.
- [8] Turányi, T., and Tomlin, A. S., *Analysis of Kinetic Reaction Mechanisms*, Springer-Verlag, New York, 2014.
- [9] Peters, N., and Williams, F., "The Asymptotic Structure of Stoichiometric Methane-Air Flames," *Combustion and Flame*, Vol. 68, No. 2, 1987, pp. 185–207.
- [10] Rogg, B., and Peters, N., "The Asymptotic Structure of Weakly Strained Stoichiometric Methane-Air Flames," *Combustion and Flame*, Vol. 79, No. 3, 1990, pp. 402–420.
- [11] Tham, Y., Bisetti, F., and Chen, J.-Y., "Development of a Highly Reduced Mechanism for Iso-Octane HCCI Combustion with Targeted Search Algorithm," *Journal of Engineering for Gas Turbines and Power*, Vol. 130, No. 4, 2008, Paper 042804.
- [12] Franzelli, B., Riber, E., Sanjosé, M., and Poinso, T., "A Two-Step Chemical Scheme for Kerosene-Air Premixed Flames," *Combustion and Flame*, Vol. 157, No. 7, 2010, pp. 1364–1373.
- [13] Boivin, P., Jiménez, C., Sánchez, A. L., and Williams, F. A., "An Explicit Reduced Mechanism for H₂-Air Combustion," *Proceedings of the Combustion Institute*, Vol. 33, No. 1, 2011, pp. 517–523.
- [14] Xin, Y., Sheen, D. A., Wang, H., and Law, C. K., "Skeletal Reaction Model Generation, Uncertainty Quantification and Minimization: Combustion of Butane," *Combustion and Flame*, Vol. 161, No. 12, 2014, pp. 3031–3039.
- [15] Lam, S., and Goussis, D., "The CSP Method for Simplifying Kinetics," *International Journal of Chemical Kinetics*, Vol. 26, No. 4, 1994, pp. 461–486.
- [16] Lu, T., and Law, C. K., "A Directed Relation Graph Method for Mechanism Reduction," *Proceedings of the Combustion Institute*, Vol. 30, No. 1, 2005, pp. 1333–1341.
doi:10.1016/j.proci.2004.08.145
- [17] Pepiot-Desjardins, P., and Pitsch, H., "An Efficient Error-Propagation-Based Reduction Method for Large Chemical Kinetic Mechanisms," *Combustion and Flame*, Vol. 154, No. 1, 2008, pp. 67–81.
- [18] Lu, T., and Law, C. K., "Strategies for Mechanism Reduction for Large Hydrocarbons: n-Heptane," *Combustion and Flame*, Vol. 154, No. 1, 2008, pp. 153–163.
- [19] Løvås, T., "Automatic Generation of Skeletal Mechanisms for Ignition Combustion Based on Level of Importance Analysis," *Combustion and Flame*, Vol. 156, No. 7, 2009, pp. 1348–1358.
- [20] Jaouen, N., Vervisch, L., Domingo, P., and Ribert, G., "Automatic Reduction and Optimisation of Chemistry for Turbulent Combustion Modelling: Impact of the Canonical Problem," *Combustion and Flame*, Vol. 175, Jan. 2017, pp. 60–79.
doi:10.1016/j.combustflame.2016.08.030
- [21] Smith, G. P., Golden, D. M., Frenklach, M., Moriarty, N. W., Eiteneer, B., Goldenberg, M., Bowman, C. T., Hanson, R. K., Song, S., Gardiner, W. C., Lissianski, V. V., and Qin, Z., "GRI-Mech 3.0," Gas Research Inst., Chicago, IL, 1999, http://www.me.berkeley.edu/gri_mech/ [retrieved Nov. 2016].
- [22] Lu, T., and Law, C. K., "Linear Time Reduction of Large Kinetic Mechanisms with Directed Relation Graph: n-Heptane and Iso-Octane," *Combustion and Flame*, Vol. 144, No. 1, 2006, pp. 24–36.
doi:10.1016/j.combustflame.2005.02.015
- [23] Lu, T., and Law, C. K., "On the Applicability of Directed Relation Graphs to the Reduction of Reaction Mechanisms," *Combustion and Flame*, Vol. 146, No. 3, 2006, pp. 472–483.
doi:10.1016/j.combustflame.2006.04.017
- [24] Vagelopoulos, C., and Egolfopoulos, F., "Laminar Flame Speeds and Extinction Strain Rates of Mixtures of Carbon Monoxide with Hydrogen, Methane, and Air," *Symposium (International) on Combustion Proceedings*, Vol. 25, No. 1, 1994, pp. 1317–1323.
doi:10.1016/S0082-0784(06)80773-3
- [25] Vagelopoulos, C., and Egolfopoulos, F., "Direct Experimental Determination of Laminar Flame Speeds," *Symposium (International) on Combustion Proceedings*, Vol. 27, No. 1, 1998, pp. 513–519.
doi:10.1016/S0082-0784(98)80441-4
- [26] Tahtouh, T., Halter, F., and Mounaim-Rousselle, C., "Measurement of Laminar Burning Speeds and Markstein Lengths Using a Novel Methodology," *Combustion and Flame*, Vol. 156, No. 9, 2009, pp. 1735–1743.
doi:10.1016/j.combustflame.2009.03.013
- [27] Bosschaart, K., and de Goey, L., "The Laminar Burning Velocity of Flames Propagating in Mixtures of Hydrocarbons and Air Measured with the Heat Flux Method," *Combustion and Flame*, Vol. 136, No. 3, 2004, pp. 261–269.
doi:10.1016/j.combustflame.2003.10.005
- [28] Kee, R. J., Grcar, J. F., Smooke, M., Miller, J., and Meeks, E., "PREMIX: A Fortran Program for Modeling Steady Laminar One-Dimensional Premixed Flames," Sandia National Lab. Rept. SAND85-8249, Albuquerque, NM, 1985.
- [29] Pitsch, H., "FlameMaster, a C++ Computer Program for 0-D Combustion and 1-D Laminar Flame Calculations," Institut für Technische Verbrennung, Aachen, Germany, 1998, <https://www.itv.rwth-aachen.de/index.php?id=flamemaster&L=1> [retrieved Nov. 2016].
- [30] Desjardins, O., Blanquart, G., Balarac, G., and Pitsch, H., "High Order Conservative Finite Difference Scheme for Variable Density Low Mach Number Turbulent Flows," *Journal of Computational Physics*, Vol. 227, No. 15, 2008, pp. 7125–7159.
doi:10.1016/j.jcp.2008.03.027
- [31] Kee, R. J., Rupley, F. M., and Miller, J. A., "Chemkin-II: A Fortran Chemical Kinetics Package for the Analysis of Gas-Phase Chemical Kinetics," Sandia National Lab. TR SAND89-8009B, Albuquerque, NM, 1991.
- [32] Attili, A., Bisetti, F., Mueller, M. E., and Pitsch, H., "Effects of Non-Unity Lewis Number of Gas-Phase Species in Turbulent Nonpremixed Sooting Flames," *Combustion and Flame*, Vol. 166, April 2016, pp. 192–202.
doi:10.1016/j.combustflame.2016.01.018
- [33] Cooke, J. A., Bellucci, M., Smooke, M. D., Gomez, A., Violi, A., Faravelli, T., and Ranzi, E., "Computational and Experimental Study of JP-8, a Surrogate, and Its Components in Counterflow Diffusion Flames," *Proceedings of the Combustion Institute*, Vol. 30, No. 1, 2005, pp. 439–446.
doi:10.1016/j.proci.2004.08.046
- [34] Jomaas, G., Zheng, X., Zhu, D., and Law, C., "Experimental Determination of Counterflow Ignition Temperatures and Laminar Flame Speeds of C₂-C₃ Hydrocarbons at Atmospheric and Elevated Pressures," *Proceedings of the Combustion Institute*, Vol. 30, No. 1, 2005, pp. 193–200.
doi:10.1016/j.proci.2004.08.228
- [35] Pitsch, H., "Large-Eddy Simulation of Turbulent Combustion," *Annual Review of Fluid Mechanics*, Vol. 38, Jan. 2006, pp. 453–482.
doi:10.1146/annurev.fluid.38.050304.092133
- [36] Bisetti, F., Blanquart, G., Mueller, M., and Pitsch, H., "On the Formation and Early Evolution of Soot in Turbulent Nonpremixed Flames," *Combustion and Flame*, Vol. 159, No. 1, 2012, pp. 317–335.
doi:10.1016/j.combustflame.2011.05.021
- [37] Passot, T., and Pouquet, A., "Numerical Simulation of Compressible Homogeneous Flows in the Turbulent Regime," *Journal of Fluid Mechanics*, Vol. 181, Aug. 1987, pp. 441–466.
doi:10.1017/S0022112087002167
- [38] Sankaran, R., Hawkes, E. R., Yoo, C. S., and Chen, J. H., "Response of Flame Thickness and Propagation Speed Under Intense Turbulence in Spatially Developing Lean Premixed Methane-Air Jet Flames," *Combustion and Flame*, Vol. 162, No. 9, 2015, pp. 3294–3306.
doi:10.1016/j.combustflame.2015.05.019
- [39] Luca, S., Attili, A., and Bisetti, F., "Direct Numerical Simulation of Turbulent Lean Methane-Air Bunsen Flames with Mixture Inhomogeneities," *54th AIAA Aerospace Sciences Meeting, AIAA SciTech*, AIAA Paper 2016-0189, 2016.
doi:10.2514/6.2016-0189
- [40] Filatyev, S. A., Driscoll, J. F., Carter, C. D., and Donbar, J. M., "Measured Properties of Turbulent Premixed Flames for Model Assessment, Including Burning Velocities, Stretch Rates, and Surface Densities," *Combustion and Flame*, Vol. 141, No. 1, 2005, pp. 1–21.
doi:10.1016/j.combustflame.2004.07.010